9^{th} *International Conference on* HYDROELASTICITY IN MARINE TECHNOLOGY
Rome, Italy, July 10^{th}-13^{th} *2022*

Experimental and Numerical Investigation of a Vertical Pre-tensioned Membrane Sheet in Regular Waves

Mukhlas, M.[1,*] Kristiansen, T.[1], Lader, P.F.[1] and Kristiansen, D.[1]

[1] Department of Marine Technology, Norwegian University of Science and Technology (NTNU), Trondheim, Norway

Abstract. A vertical pre-tensioned rectangular membrane sheet in regular waves is investigated in the present study. A two-dimensional study is carried out in a glass-wall wave flume at the Marine Technology Centre in Trondheim. The membrane is fixed at the flume's bottom and attached to vertical and horizontal springs at the top. A linearized frequency-domain analysis using the framework of generalized body modes is performed in WAMIT v7.3. The wet eigenperiods are predicted reasonably well by the numerical model. The horizontal force results suggest the importance of viscous drag force at membrane resonance periods. This might come from the flow separation at the side and bottom gaps between the membrane sheet and the flume walls in the experiment. The generalized drag force based on the Morison equation is added to the system of equations, and the unknown membrane motion is solved in the time domain. The inclusion of drag force demonstrates some improvement to the results, although they need further research.

Key words: *Hydroelasticity; Membrane; Gravity waves; Two-dimensional*

1. Introduction

Several concepts of ocean structures, in which the membrane is the main constituent of the constructions, have been proposed in recent years. Some examples are closed flexible bag for aquaculture [1, 2, 3], floating membrane solar island [4, 5], membrane breakwater [6], floating fluid-filled membrane barge [7], and submerged fluid-filled membrane breakwater [8]. One of the main arguments for using membrane for structures in an ocean environment is its flexibility; hence the structural loads can be dramatically reduced in comparison to rigid structures with similar geometrical shapes. However, this adds another difficulty in predicting the hydrodynamic response of such structures under wave loads since the hydrodynamic loads, the structural loads, and the structures' responses are coupled. In addition, based on the authors' previous experience on the closed flexible bag for aquaculture in [1, 3], the membrane responses in waves give two main identified challenges to the structures: snap loads on the membrane and mean heave set-down. Stress concentrations in connections have also been addressed as the main challenge. Hence, more knowledge of the membrane responses in waves is the first necessary step in understanding the problem.

The present study investigates a near two-dimensional vertical pre-tensioned membrane in regular waves, focusing on membrane responses and loads. The study is intended as a groundwork for rational structural and hydrodynamic modeling of the closed flexible bag, where the two-dimensional problems introduced in [9, 10] have inspired the authors to study their membrane system using experimental and numerical methods. The motivation for a two-dimensional study is to have a more controlled study of

*Correspondence to: muhammad.mukhlas@ntnu.no

the system's physics, and it is also easier to perform a parameter sensitivity study. The experimental setup, data analysis, and errors discussion are presented in Section 2. A numerical method based on generalized modes of body motion [11, 12] is adopted and is explained briefly in Section 3; the total deformation of the membrane is expressed as a sum of the membrane's dry eigenmodes. Consequently, the membrane is assumed to be governed by the linear membrane equation; hence, it limits the method to a small deformed membrane slope and small dynamic tension. Experimental and numerical results are presented in Section 4, and possible candidates that cause the differences are addressed and discussed. One important finding that needs to be emphasized is the experimental bias errors resulting from the three-dimensionality of membrane motions and viscous gap flow between the membrane and the flume's glass wall. In particular, it was found that the flow separation at those gaps was so dominant, inducing significant viscous damping and excitation forces to the membrane system. Therefore, it is not recommended to do similar two-dimensional membrane studies in the future.

2. Model tests

2.1. Experimental setup

A schematic drawing of the model test setup is given in Fig. 1. The model tests were conducted in a glass-wall wave flume at the Marine Technology Centre in Trondheim. The wave flume is 13.64 m long and 0.60 m wide, with water depth $h = 1.0$ m. The wave flume is equipped with one bottom-hinged wavemaker (WM) located at $x = -7.0$ m and one parabolic beach at x = 6.0 m. In addition, six wave probes (WP1-WP6) of capacitance type were distributed inside the flume to measure the free-surface elevation.

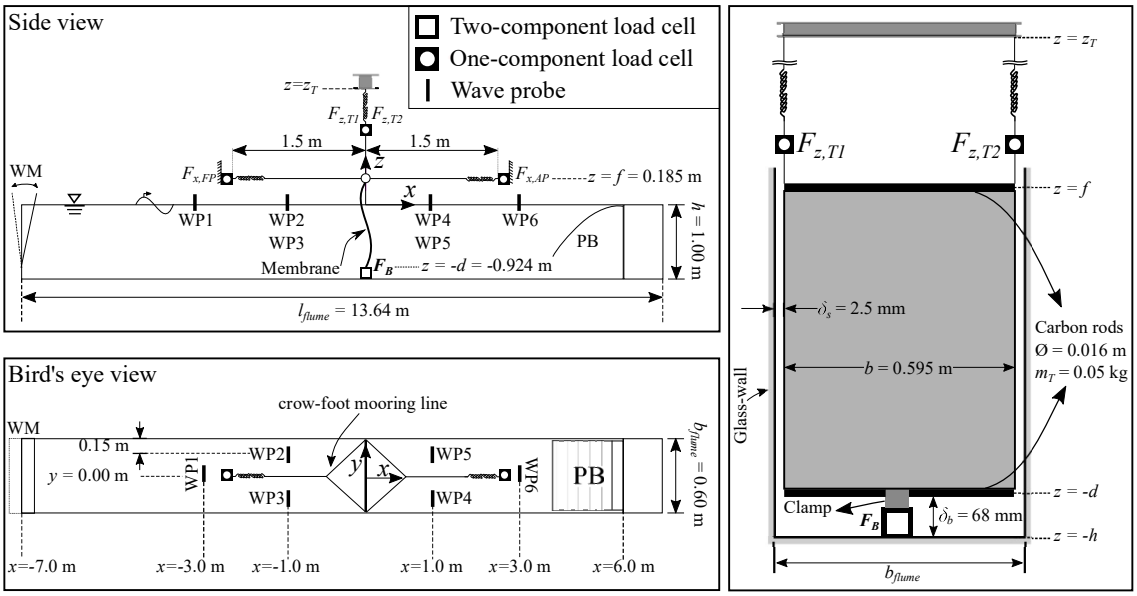

Figure 1: Schematic drawing of the experimental setup. Top-left: side view of the setup. Bottom-left: bird's eye view of the setup. Right: front view of the membrane. A wavemaker (WM) and a parabolic beach (PB) are located on the flume's ends. The membrane is located approximately at the middle of the flume (i.e., at $x = 0$ m), and the details of the attachments are provided in the right part of the figure. The locations of the wave probes (WP1-WP6), and the load cells ($\mathbf{F_B}$, $F_{x,FP}$, $F_{x,AP}$, $F_{z,T1}$, and $F_{z,T2}$) are given. Different membrane pre-tension values were achieved by varying the vertical spring elongation controlled by moving the attachment point at $z = z_T$ vertically.

A rectangular membrane sheet with length $l = 1.109$ m and breadth $b = 0.595$ m was made of Ripstop nylon material with surface density of $\rho_m = 0.164$ kg/m^2. There were two narrow side gaps with a width of $\delta_s = 0.0025$ m between the membrane and the flume's glass walls as indicated in Fig. 1. The top and bottom parts of the sheet were sewn to lightweight carbon rods with a diameter of $\emptyset = 0.016$ m and mass $m_T = 0.050$ kg. The bottom rod was attached at $z = -d = -0.924$ m to two-component load cell, hence there existed a bottom gap $\delta_b = h - d + 0.5\emptyset = 0.068$ m. That load cell measured both horizontal and vertical forces at membrane bottom $\mathbf{F_B} = [F_{x,B},\, F_{z,B}]$. The top rod located at $z = f = 0.185$ m was connected to vertical lines and horizontal crow-foot mooring lines that lead to springs with stiffness $k_s = 278.37$ N/m. Tension on those lines were measured by four one-component load cells (i.e., $F_{x,FP}$, $F_{x,AP}$, $F_{z,T1}$, and $F_{z,T2}$) as indicated in Fig. 1. All measurements were acquired with a sampling frequency of $f_s = 200$ Hz, and they were low-pass filtered at 20 Hz using a Butterworth filter. Pre-tension was applied to the membrane sheet prior to each test by varying the elongation of the vertical spring, hence five different normalized pre-tension values could be tested: $\widetilde{T}_0 = \frac{T_0}{\rho g h^2 b} = [0.01, 0.0125, 0.015, 0.0175, 0.02]$, where T_0 refers to the pre-tension force (N).

In total, 964 regular wave tests were performed, including repetition tests. The regular waves had periods between $0.7 \leq T\,(s) \leq 1.5$ with period spacing of $dT = 0.02$ s, and four different wave steepnesses $\varepsilon = [1/60, 1/45, 1/30, 1/15]$. Examples of the measurements are given in Fig. 2. Wave documentation tests were also performed at the beginning of the experimental period; the membrane was not installed, and undisturbed wave elevation was measured. The measured wave amplitudes by WP1-WP6 from the wave documentation tests were 94-99% of the input wave amplitudes.

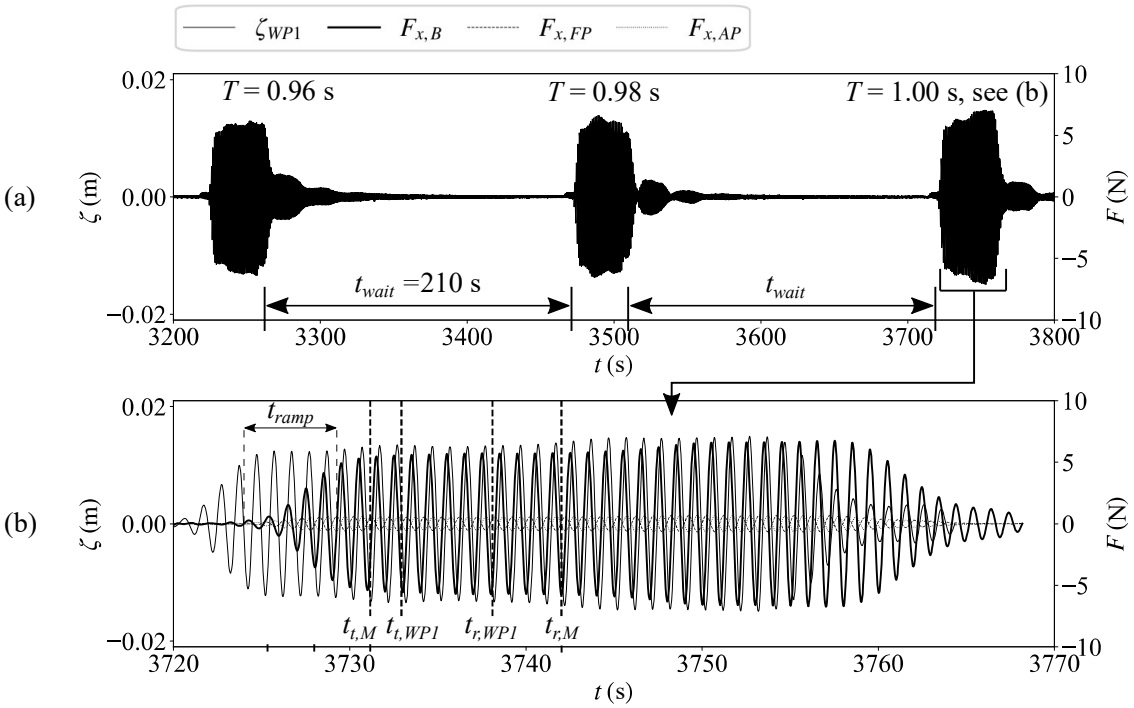

Figure 2: Example of the measurements of wave probe and horizontal forces, extracted from the tests with wave steepness $\varepsilon = 1/60$ and normalized pre-tension $\widetilde{T}_0 = 0.175$. For each test, the input signals to the wavemaker are multiplied with a cosine taper window to ramp the ends of the time series slowly for five oscillation periods (i.e., t_{ramp} = 5T). In (a), only three tests with $T = [0.96, 0.98, 1.00]$ s are presented for clarity. The waiting time t_{wait} between each test was 210 s, which was found to be sufficient to calm the water down. The zoom-in of the filtered signals for $T = 1.00$ s is presented in (b).

Experimental results presented in Section 4 are calculated from average amplitudes of the near steady-state part of the filtered time series. The signals were band-pass filtered around the basic harmonic by multiplication with a Gaussian mask in the frequency domain. An example of filtered signals and truncation of the steady-state time window is presented in Fig. 2b. For the membrane force measurements, the steady-state parts were determined as time windows between the end of the start-up transient stage $t_{t,M}$ and the arrival of wave re-reflections $t_{r,M}$. Typically, the membrane required two oscillation periods after ramp-up to reach the steady-state; hence $t_{t,M} = 1.4t_{ramp}$ was used. This is illustrated in Fig. 2 for $F_{x,B}$ measurement. $t_{r,M}$ was estimated based on the minimum time between the re-reflected waves from the wavemaker or the beach reaching the membrane again. All the aforementioned time quantities were estimated based on linear wave group velocity C_g for finite water depth. A similar principle also applies to estimate the end time of wave probes' steady-state windows. However, for the start time of wave probes' steady-state windows (e.g., $t_{t,WP1}$ for WP1 in Fig. 2), it was estimated as the time when reflected/transmitted waves by the membrane reached the wave probes.

2.2. Brief discussion on error sources

The wave re-reflections were important error sources since they limited the number of oscillations in the extracted steady-state windows. For example, less than five steady-state oscillations typically could be extracted for $T > 1.20$ s. This might affect the accuracy when extracting the amplitudes at membrane resonance periods, for instance, since the responses might still gradually build up towards steady-state amplitudes. However, due to rather large relative damping, all results are considered reasonable.

Four repetition tests were performed to quantify random errors in the experiment. Hence, five samples were available to quantify the random errors. Due to the limited amount of time, the repetition tests only covered membrane pre-tension $\widetilde{T}_0 = 0.0175$, the same wave period range and wave steepnesses, but with a period spacing of $dT = 0.10$ s. The maximum relative standard deviation (RSD) for the basic harmonic component of measured horizontal forces and wave elevations was 7.33%, which was within typical experimental error levels. However, large RSD up to 50.81% was found for the basic harmonic component of the vertical membrane force. Their basic harmonic component was typically around 2% of the pre-tension force. Hence, the membrane was very stiff longitudinally, and it is not of present interest to investigate the oscillating component of vertical force.

Another source of errors that could not be reflected in the repetition tests was bias errors. One source of bias error was the standing wave modes of the flume. The first longitudinal mode (i.e., seiching) had a different time scale (≈ 8.79 s) than the tested wave periods; hence it could be mitigated by the applied band-pass filter and the waiting time t_{wait}. The first transverse mode eigenperiod (≈ 0.88 s) was within the tested wave periods, which could be triggered by slight three-dimensionality of the membrane motions causing three-dimensional fluid behavior inside the flume. It was observed that the membrane showed somewhat three-dimensional twisting-like motion (i.e., approximately 180° phase difference between motion about z-axis) near the bottom rod at $z = -d$. The last source of bias error was the sides and bottom gaps between the membrane and the flume (see Fig. 1), which was found to be significant and is discussed further in Sections 3 and 4. In fact, this effect was so dominant, that it is not recommended to do similar "2D" membrane studies in the future.

3. Numerical method

A numerical method based on potential flow theory and linearized membrane equation was adopted to analyze the experimental results in Section 2. Fig. 3 illustrates the two-dimensional problem definition of the model test in Section 1. Solutions of the fluid flow (i.e., velocity vector $\nabla\phi(x, y, z, t)$ and pressure fields $p(x, y, z, t)$) can be calculated by velocity potential ϕ that satisfies the following boundary value problem (BVP)

$$\nabla^2\phi = \quad 0, \qquad \text{in } \Omega_0 \tag{1}$$

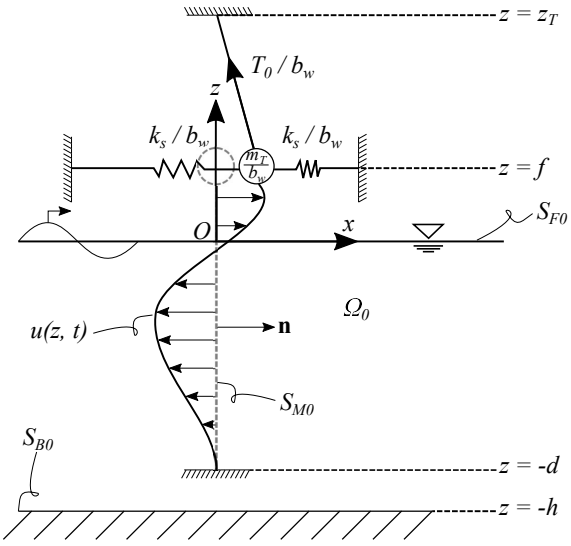

Figure 3: Problem and coordinate system definition of the vertical pre-tensioned membrane sheet in waves. A Cartesian coordinate system Oxz with the origin at the mean water level (MWL) is employed. Time-varying oscillation of membrane deformation is described by $u(z,\, t)$. The normal vector $\mathbf{n}$ is defined to point to the mean position of the membrane surface S_{M0}.

$$\frac{\partial \phi}{\partial z} = -\frac{1}{g}\frac{\partial^2 \phi}{\partial t^2}, \quad \text{on } S_{F0} \tag{2}$$

$$\frac{\partial \phi}{\partial z} = 0, \quad \text{on } S_{B0} \tag{3}$$

$$\nabla \phi \cdot \mathbf{n} = \mathbf{V} \cdot \mathbf{n}, \quad \text{on } S_{M0} \tag{4}$$

where S_{F0}, S_{B0}, and S_{M0} define the mean boundary positions of the free-surface, sea bottom, and membrane, respectively. A radiation condition of radiated waves is imposed on the far-field to complete the BVP. Generalized body modes feature in WAMIT v7.3 [11, 12] was used to solve the BVP. The membrane was discretized into quadrilateral long dipole panels with breadth $b_W = 16d$. Consequently, the three-dimensional effect was minimum. Hence, the obtained hydrodynamic quantities from WAMIT needed to be multiplied by a factor $b \,/\, b_W$ to be consistent with the model tests. Numerical studies with channel wall effects for both source and dipole panels were also attempted, but without any success. Comparing the three numerical approaches with the results of two-dimensional numerical studies in [9, 10] (not shown), a satisfactory agreement was obtained only for the long dipole panels without wall effects. Also, several convergence error messages were obtained when the channel width was of the same order as the body. More dedicated numerical studies are required to investigate the channel wall effects on the present model tests.

The membrane motion $u(z,\, t)$ is assumed to be two-dimensional, which obeys the following linear membrane equation

$$\rho_m \frac{\partial^2 u}{\partial t^2} - \frac{T_0}{b_W}\frac{\partial^2 u}{\partial z^2} = p(y, z, t) \tag{5}$$

where the term on the right-hand side represents the fluid pressure acting on S_{M0}. The corresponding membrane boundary conditions in Fig. 3 are

$$u(-d,\, t) = 0 \tag{6}$$

$$T_0 \frac{\partial u}{\partial z}(f,\, t) + \left\{2k_s + \frac{T_0}{z_T - f}\right\} u(f,\, t) = 0 \tag{7}$$

The top boundary condition in Eq. 7 is derived based on the horizontal equilibrium of *massless* mass-spring system at $z = f$. From a numerical trial study, added-mass force acting on the membrane was found to be larger than the rod's mass m_T by thousandfolds. Hence it is reasonable to neglect rod's inertial force.

Since the governing equation and the boundary conditions are linear and homogeneous, the solutions can be found using the method of separation of variable. The homogeneous solutions of $u(z,\, t)$ can be written as

$$u(z,t) = \sum_{j=1}^{\infty} D_j(t) f_j(z) = Re\left\{ \sum_{j=1}^{\infty} \xi_j f_j(z) e^{i\omega t} \right\},\ \xi_j \in \mathbb{C} \tag{8}$$

where the unknown time-dependent constants $D_j(t)$ are assumed to oscillate with basic harmonic (i.e., $D_j(t) \propto e^{i\omega t}$) with complex amplitude ξ_j. The second term in the right-hand side of Eq. 8 represents the eigenfunctions $f_j(z) = \sin \lambda_j(z + d)$, on which the eigenvalues λ_j are found through boundary conditions in Eqs. 6 and 7. The normal velocity component of arbitrary point within the membrane in Eq. 4 can then be written as

$$\mathbf{V} \cdot \mathbf{n} = \underbrace{\left[\sum_{j=1}^{\infty} i\omega \xi_j f_j(z) e^{i\omega t},\, 0,\, 0 \right]}_{\mathbf{V}} \cdot \underbrace{[n_x,\, 0,\, 0]}_{\mathbf{n}} = \sum_{j=1}^{\infty} i\omega \xi_j \underbrace{f_j(z)\, n_x}_{n_j} e^{i\omega t} \tag{9}$$

Eq. 9 above was used as an input to solve the radiation problem in WAMIT.

After solving the BVP for the unknown velocity potential ϕ, the hydrodynamic pressure p in Eq. 5 can be obtained using the linear Bernoulli equation. A set of equations of motion can be obtained by multiplying Eq. 5 by eigenfunctions f_i and integrating the resulting equation over the mean membrane length l (see [11] for details)

$$\sum_{j=1}^{\infty} \left\{ -\omega^2 (M_{ij} + a_{ij}(\omega)) + i\omega b_{ij}(\omega) + (C_{ij} + c_{ij}) \right\} \xi_j = X_i(\omega) \tag{10}$$

where

$$M_{ij} = \rho_m b_W \int_{-d}^{f} f_i f_j \, dz, \text{ and } C_{ij} = T_0 \lambda_j^2 \int_{-d}^{f} f_i f_j \, dz, \text{ respectively.} \tag{11}$$

a_{ij}, b_{ij}, c_{ij}, and X_i in Eq. 10 are the added mass coefficients, wave damping coefficients, hydrostatic restoring coefficients, and wave-exciting forces, respectively. Finally, the membrane motion $u(z, t)$ at each wave frequency ω can be determined from Eqs. 8 and 10. The corresponding horizontal forces at top $F_{x,T}$ (N) and bottom $F_{x,B}$ (N) of the membrane can be calculated by

$$F_{x,T} = T_0 \frac{\partial u}{\partial z}|_{z=f}, \text{ and } F_{x,B} = T_0 \frac{\partial u}{\partial z}|_{z=-d} \tag{12}$$

As a pragmatic attempt to include viscous drag force, the drag part of the Morison equation is applied stripwise along the membrane length. The mean wetted part of the membrane is divided into N strips with length Δz and breadth b, and the cross-flow drag force is applied to each membrane strip at vertical coordinate $z = z_n$. Following the same approach committed to obtain Eq. 10, the generalized Morison drag force $F_{D,i}$ can then be written as

$$F_{D,i} = \sum_{n=1}^{N} \frac{\rho C_D b}{2} \underbrace{(u_w(u(z_n,t), z_n, t) - \dot{u}(z_n,t))}_{u_r} |u_w(u(z_n,t), z_n, t) - \dot{u}(z_n,t)|\, f_i(z_n) \Delta z \tag{13}$$

where C_D, u_w, and u_r are drag coefficient, undisturbed horizontal wave particle velocity, and relative horizontal velocity between membrane strip and the undisturbed wave-particle, respectively. Note that

the u_w is estimated at the exact horizontal position of the membrane strip; hence it is a function of the total membrane deformation $u(z_n, t)$. With the additional drag force term, the membrane equations of motion now become

$$\sum_{j=1}^{J} \Big\{ (M_{ij} + a_{ij}(\omega))\ddot{D}_j + b_{ij}(\omega)\dot{D}_j + (C_{ij} + c_{ij})D_j \Big\} = X_i(\omega)\, e^{i\omega t} + F_{D,i} \tag{14}$$

The system of equations above needs to be solved in the time domain. Runge-Kutta fourth-order scheme is implemented to solve the initial value problem of the time-dependent constants D_j, $\dot{D}_j$, and $\ddot{D}_j$. The time-history prior to steady-state does not have physical significance; it is only the steady-state part that is used.

It is an open question regarding the applicable C_D coefficient used in Eq. 13. It is not possible to apply Graham C_D formula [13] in this case since the flume's glass walls effects are dominant. Another way is to think of the membrane strip as a slatted screen with a solidity ratio S_n. At each membrane strip, the corresponding pressure-drop coefficient can be calculated using the Baines–Peterson–Weisbach formula presented in [14, 15] (see e.g. [16] for the formula application in moonpool damping). The formula assumes the pressure drop coefficient as a function of S_n, and it does not depend on the Keulegan-Carpenter number KC. However, for present study, the solidity ratio of the membrane strip is S_n = 0.99, and the formula might not be accurate for S_n >0.90 [17]. Putting S_n = 0.99 into the formula would yield overly large C_D = 41520. In addition, the membrane strips are flexible; hence when three-dimensional membrane motion occurs (e.g., twisting motion as described in Section 2.2), the corresponding local tension changes might affect the drag force on the strip and its neighboring strips. Consequently, this limits the applicability of Eq. 14. Hence, in principle, the problem in the present study has to be solved as a three-dimensional hydroelastic problem in viscous fluid flow. Therefore, the viscous drag in the present study is included purely by using heuristic drag-coefficient.

4. Results and discussions

A comparison of numerical and experimental horizontal force amplitudes for three different membrane pre-tension values $\widetilde{T}_0 = [0.0125, 0.0175, 0.0200]$ is presented in Fig. 4. The numerical results are calculated based on small steepness waves assumption with correspondingly small membrane slope $\frac{\partial u}{\partial z}$ as presented in Section 3, which might not necessarily be valid when the membrane has a large motion amplitude $u(z, t)$ (e.g., at resonance) and hence requires in-plane membrane dynamic to be solved in addition. Nevertheless, the membrane wet eigenperiods are predicted reasonably well by the numerical results but with an apparent discrepancy in the force amplitudes. A fair agreement between the numerical and experimental results can be observed outside the resonance period. The experimental and numerical results show that the effect of increasing membrane pre-tension is to decrease the wet eigenperiods and reduce the maximum horizontal forces, respectively. Note that the force peaks are, in principle, not necessarily coinciding with the wet modal eigenperiods, since they depend on phasing between modes (see Eqs. 8 and 12). However, for all the analyzed cases, it was found that the force peaks occurred in the vicinity of wet modal eigenperiods.

A qualitative comparison of membrane maximum deformation between the experimental and numerical results is presented in Fig. 5. Based on video snapshots during the experiments, WAMIT predicts membrane deformation qualitatively well. Furthermore, the wavefield amplitude and phase prediction in the vicinity of the membrane are also in good agreement with the experiment. However, it is apparent that the membrane motion was not uniform in the y-direction, where some qualitative illustrations of the observed three-dimensional motion are given in the figure. One of the examples is the discussed twisting motion in Section 2.2, which is present in the experimental snapshot at $T = 0.96$ s. Hence, Eq. 5 could not totally explain the membrane responses in the experiment, and the three-dimensional membrane equation, together with channel wall effects, would be needed to solve the problem.

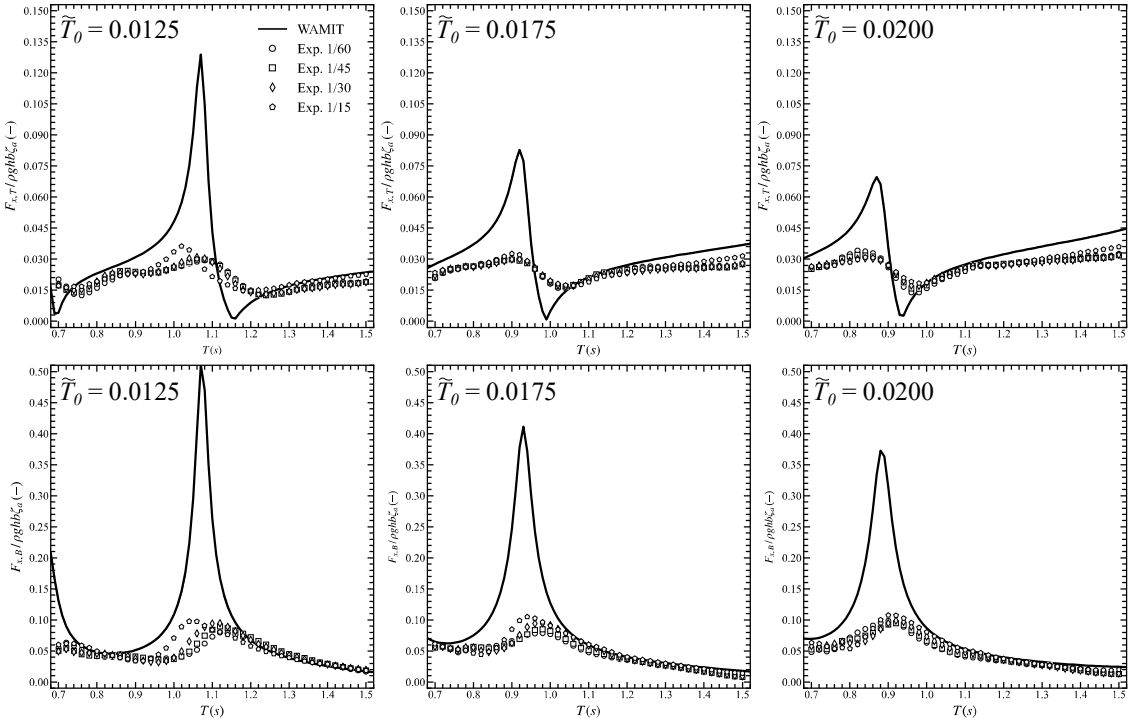

Figure 4: Overview of the horizontal force amplitude between experiment and numerical results. First row: normalized horizontal force at membrane top. Second row: normalized horizontal force at membrane bottom. Note the different scales between the first and the second row.

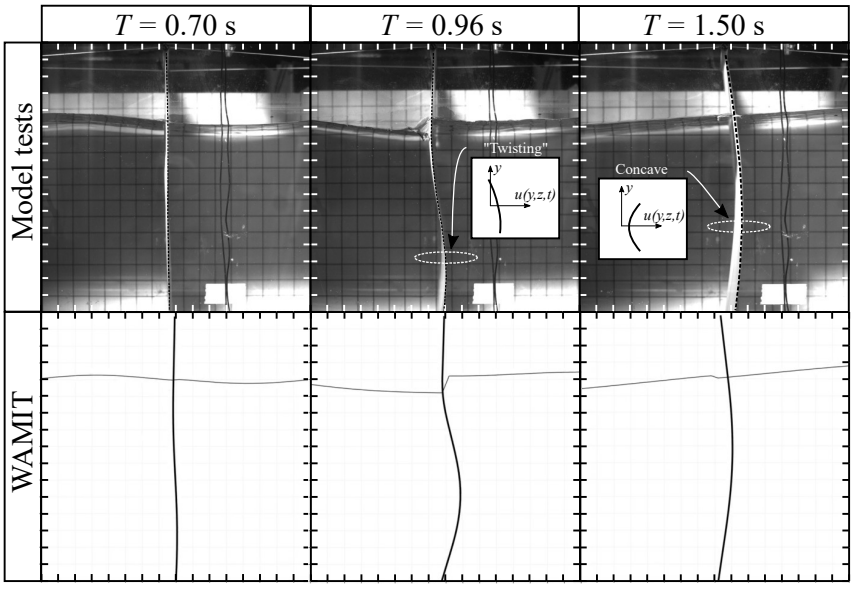

Figure 5: A qualitative comparison of membrane maximum deformation between experimental and numerical results. The presented snapshots are from the case with $\widetilde{T}_0$ = 0.0175, T = [0.70, 0.96, 1.50] s and ε = 1/30.

One candidate that might explain the amplitude discrepancy in Fig. 4 is the significant viscous drag force from the side and bottom gaps, as discussed in Section 2.2 and Section 3. The numerical results that include the Morison drag force are given in Fig. 6, where only the case with $\widetilde{T}_0 = 0.0125$ is presented for clarity. The drag coefficient is assumed as C_D = 20. With the inclusion of drag force, it is apparent that the viscous damping increases at resonance with increasing wave steepness. However, the experimental horizontal bottom force results say otherwise. The results suggest that viscous excitation is of importance at resonance. The simplified drag model has not captured this. It is possible that a more complete model would improve this, where using diffracted wave particle velocity rather than the undisturbed incident wave particle velocity would be a possibly important ingredient. However, in order to proceed in this direction, one would need to solve a coupled system between the incident waves, diffracted waves, and viscous gap flow. Further, the membrane twisting motion would also need to be included, turning the problem into a full three-dimensional one. Hence, it was decided not to follow this path, since it became clear at that stage that the attempt to perform a two-dimensional model test as a part of a more complex three-dimensional problem was not successful.

Another candidate is that the effective membrane pre-tension increases for more significant membrane motion. The experimental horizontal force results in Fig. 6 clearly show a shift of resonance peak to lower wave period with increasing wave steepness. The shift can also be observed in Fig. 4 for the other two pre-tension values, and it is apparent that the shift is more prominent with decreasing membrane pre-tension. This fact is supported by the mean vertical force measurements in the steady-state time window, on which the mean force amplitudes normalized by the pre-tension are presented in Fig. 7. From Fig. 7, it can be seen that the mean vertical force amplitudes increase with increasing wave steepness and decreasing pre-tension. For $\widetilde{T}_0 = 0.0125$, up to $7 - 8\%$ increase of pre-tension can be observed for wave steepness $\varepsilon = 1/15$. This means that the wet eigenperiod for $\varepsilon = 1/15$ should be approximately proportional with the inverse square root of the effective pre-tension (i.e., $(1.07T_0)^{-1/2}$). This yields approximately 4% shift of the resonance period from $T_{n,1/60}$ to $T_{n,1/15}$, which is of the same order as the shift of the experimental force peaks in those two wave steepness cases.

5. Conclusions

A rectangular membrane sheet in regular waves is investigated in the present study. The main motivation of the present paper was to study the membrane in a two-dimensional setting and perform a parameter sensitivity study on the membrane responses under different wave parameters and different pre-tension. A linearized frequency-domain analysis using the framework of generalized body modes was performed in WAMIT v7.3. Furthermore, the horizontal and vertical forces at the top and bottom of the membrane were studied, and the numerical and experimental results of membrane deformation were qualitatively compared.

Experimental and numerical horizontal force amplitudes show significant discrepancies at resonance periods but with a fair agreement outside those periods. The results suggest that the experimental bias errors from the three-dimensionality of membrane motions and viscous gap flow were so large that they significantly affected the membrane response at resonance periods. Stripwise Morison drag formula was included in the membrane system of equations as an attempt to explain the discrepancies. The calculation results with the additional drag term show a clear improvement, mainly in the damping part, but still with considerable deviation from the experimental results. Also, only a pure heuristic C_D was chosen due to the lack of experimental data for this situation in the literature. Ultimately, the present problem would require a complete three-dimensional hydroelastic formulation of the membrane and the viscous flow and channel wall effects. Hence, the attempt to perform a two-dimensional model test as a part of a more complex three-dimensional problem was not successful.

In addition, it was observed from the experimental results that the resonance periods shifted to the lower wave periods with increasing wave steepness. This can be explained by the increasing membrane effective pre-tension when significant membrane motion occurs; hence the shift was more apparent in

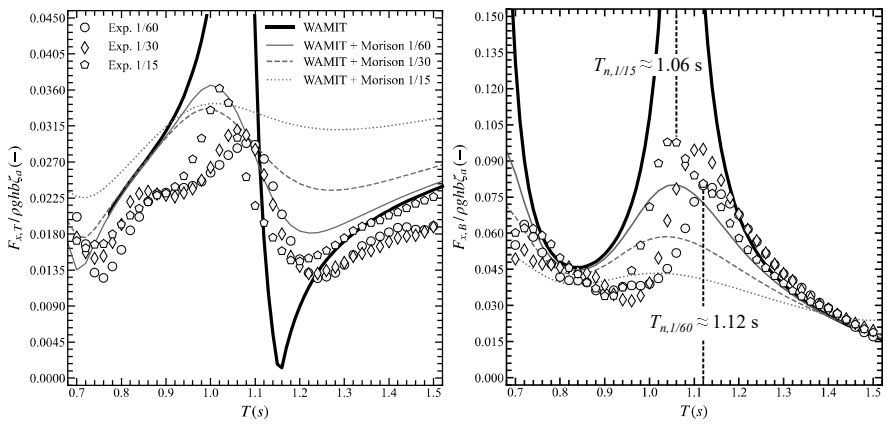

Figure 6: Normalized horizontal force amplitude (zoom-in view) for the case with $\widetilde{T}_0 = 0.0125$. Left: normalized horizontal force at membrane top. Right: normalized horizontal force at membrane bottom. The corresponding numerical results that include Morison drag force are also presented. $T_{n,1/60}$ and $T_{n,1/15}$ indicate the observed horizontal force peak amplitudes from the experiment with wave steepness $\varepsilon = 1/60$ and $1/15$, respectively.

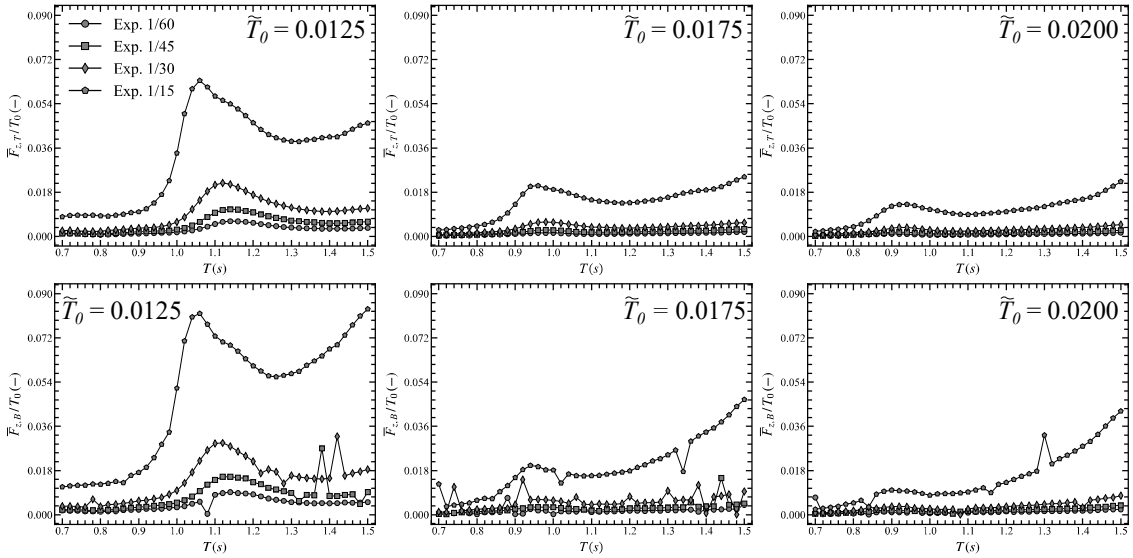

Figure 7: Measured mean vertical force amplitudes in the experiment. First row: normalized mean vertical force at membrane top. Second row: normalized mean vertical force at membrane bottom. Each column presents the results for different membrane pre-tension values. The outliers in the $\overline{F}_{z,B}/T_0$ are due to the sensor drift, which typically occurs when the sensor is submerged in the water.

the membrane with lower pre-tension values. For the lowest presented pre-tension value and the highest wave steepness (i.e., $\widetilde{T}_0 = 0.0125$ and $\varepsilon = 1/15$), up to $7 - 8\%$ increase of pre-tension was suggested by the mean vertical force measurements. This yields approximately 4% shift of resonance to a lower wave period, which is of the same order as the shift in experimental force peaks.

Acknowledgments

This work was parly supported by the Research Council of Norway through SFI Blues, grant number 309281.

References

[1] P. Lader, D. W. Fredriksson, Z. Volent, J. DeCew, T. Rosten and I. M. Strand. *Wave response of closed flexible bags*. Journal of Offshore Mechanics and Arctic Engineering, 139(051301), October 2017.

[2] I. M. Strand and O. M. Faltinsen. *Linear wave response of a 2D closed flexible fish cage*. Journal of Fluids and Structures, 87:58–83, May 2019.

[3] M. Mukhlas, P. F. Lader, D. Kristiansen, T. Kristiansen and M. Kanazawa. *Bag and floater motions of a fabric membrane cage*. Journal of Fluids and Structures, 106:103353, October 2021.

[4] T. Aas-Hansen. *Evaluation of Seakeeping Capabilities of a Floating Solar Plant*. Master's thesis, Norwegian University of Science and Technology, Trondheim, 2018.

[5] T. Kristiansen and P. Borvik. *Investigation of an Air-Cushion Supported Solar Island*. In OMAE2018, Volume 9: Offshore Geotechnics; Honoring Symposium for Professor Bernard Molin on Marine and Offshore Hydrodynamics, June 2018.

[6] G. O. Thompson, C. K. Sollitt, W. G. McDougal and W. R. Bender. *Flexible membrane wave barrier*. In Civil Engineering in the Oceans V : Proceedings of the International Conference, pages 129–148, Texas, USA, 1992.

[7] W. R. Hawthorne. *The early development of the Dracone flexible barge*. Proceedings of the Institution of Mechanical Engineers, 175(1):52–83, 1961.

[8] T. Ohyama, M. Tanaka, T. Kiyokawa, T. Uda and Y. Murai. *Transmission and reflection characteristics of waves over a submerged flexible mound*. Coastal Engineering in Japan, 32(1):53–68, July 1989.

[9] M. H. Kim and S. T. Kee. *Flexible membrane wave barrier. I: analytic and numerical solutions*. Journal of Waterway, Port, Coastal, and Ocean Engineering, 122(1):46–53, January 1996.

[10] E. Y. M. Lo. *Performance of a flexible membrane wave barrier of a finite vertical extent*. Coastal Engineering Journal, 42(2):237–251, June 2000.

[11] J. Newman. *Wave effects on deformable bodies*. Applied Ocean Research, 16(1):47–59, January 1994.

[12] C. H. Lee and J. N. Newman. *WAMIT® USER MANUAL Version 7.3*, 2019.

[13] J. M. R. Graham. *The forces on sharp-edged cylinders in oscillatory flow at low Keulegan–Carpenter numbers*. Journal of Fluid Mechanics, 97(2):331–346, 1980.

[14] W. D. Baines and E. Peterson. *An investigation of flow through screens*. Trans. Am. Soc. Mech. Engrs., 73, 1951.

[15] J. L. Weisbach. *Die experimental hydraulik*. Engelhardt, 1855.

[16] O. Faltinsen and A. Timokha. *On damping of two-dimensional piston-mode sloshing in a rectangular moonpool under forced heave motions*. Journal of Fluid Mechanics, 772:R1, 2015.

[17] O. M. Faltinsen, R. Firoozkoohi and A. N. Timokha. *Effect of central slotted screen with a high solidity ratio on the secondary resonance phenomenon for liquid sloshing in a rectangular tank*. Physics of Fluids, 23(6):062106, June 2011.